ISIJ International, Vol. 36 (1996), No. 5, pp. 603–610

Ferrite Grain Refinement by Large Reduction per Pass in Non-recrystallization Temperature Region of Austenite

Akihiko KOJIMA, Yoshiyuki WATANABE, Yoshio TERADA, Atsuhiko YOSHIE and Hiroshi TAMEHIRO[1)]

Kimitsu R & D Laboratory, Nippon Steel Corporation, Kimitsu, Kimitsu, Chiba-ken, 299-11 Japan.
1) Steel Research Laboratories, Nippon Steel Corporation, Shintomi, Futtsu, Chiba-ken, 293 Japan.

(Received on September 22, 1995; accepted in final form on November 29, 1995)

In order to clarify the effects of reduction per pass in non-recrystallization temperature region of austenite (γ) on ferrite (α) grain size of low carbon steels, isothermal hot compression tests have been performed. The hot deformations have been carried out by the constant reduction per pass of 10, 20 or 30% under the cumulative reduction of 30 or 50% in the non-recrystallization region. The α grain size is decreased about 15% with increasing the reduction per pass from 10 to 30% under the cumulative reduction of 50%. At this time, the α nucleation site density, which is defined as the number of γ grain boundaries, deformation bands and annealing twin boundaries per unit length of deformation direction, is increased about 30%. It is estimated that the increase in the α nucleation site density is caused by the increase in deformation bands. Furthermore, the number of α nuclei per unit length of γ grain boundaries is increased about 10% with increasing the reduction per pass from 10 to 30% under the cumulative reduction of 30%. It has been clarified by the calculation that the α grain refinement by the large reduction per pass is mainly caused by the increase in the α nucleation site density, which is led by the increase in deformation bands.

KEY WORDS: ferrite; austenite; grain size; grain refinement; reduction per pass; non-recrystallization temperature; hot deformation; ferrite nucleation; deformation band; annealing twin boundary; low carbon steel.

1. Introduction

In controlled rolling of low carbon steels, transformed microstructure is effectively refined by rolling in non-recrystallization temperature region of austenite (γ). Ferrite (α) grains are more refined with increasing cumulative reduction and with lowering rolling temperature in the non-recrystallization region.[1-6)] However, the effects of reduction per pass in the non-recrystallization region on α grain size have not been clarified.

Kozasu *et al.*[3,4)] showed that toughness of steels hardly depended on reduction per pass in low temperature region of γ. On the other hand, several effects with increasing reduction per pass in low temperature region of γ have been reported.[7-9)] For example, Sekine *et al.* showed that apparent γ grain boundaries, which contained γ grain boundaries and deformation bands, were increased,[7)] Kaji *et al.* showed that deformation bands were increased,[8)] and Yamaba *et al.* showed that toughness of mid thickness of thicker plates was improved[9)] with increasing reduction per pass in low temperature region of γ. In these studies,[7-9)] however, it has not been fully clarified (a) whether the steels were deformed at the non-recrystallization region, (b) whether the metallurgical effects were caused by only reduction per pass in the non-recrystallization region, (c) how the apparent γ grain boundaries and the deformation bands were measured, and (d) how transformation behavior and α grain size were varied.

In this study, the isothermal hot compression tests have been carried out in order to clarify the effects of reduction per pass in the non-recrystallization region on α grain size of low carbon steels. Especially, attention has been paid to deformation bands in γ which act as preferential α nucleation sites.

2. Experimental Procedure

Chemical compositions of steels used in this study are listed in **Table 1**. The steels contain 0.08 or 0.05 mass% carbon and 0.04 mass% niobium, furthermore steel B contains 11 mass ppm boron. Specimens are cylinders with 8 mm diameter and 12 mm height, and they were prepared from quarter thickness of continuous casting slabs of 240 mm thickness.

The specimens were deformed with the hot compres-

Table 1. Chemical compositions of steels. (mass%)

Steel	C	Si	Mn	P	S	Nb	N	B
A	0.08	0.24	1.40	0.01	0.005	0.04	0.002	—
B	0.05	0.27	1.63	0.01	0.003	0.04	0.002	0.0011

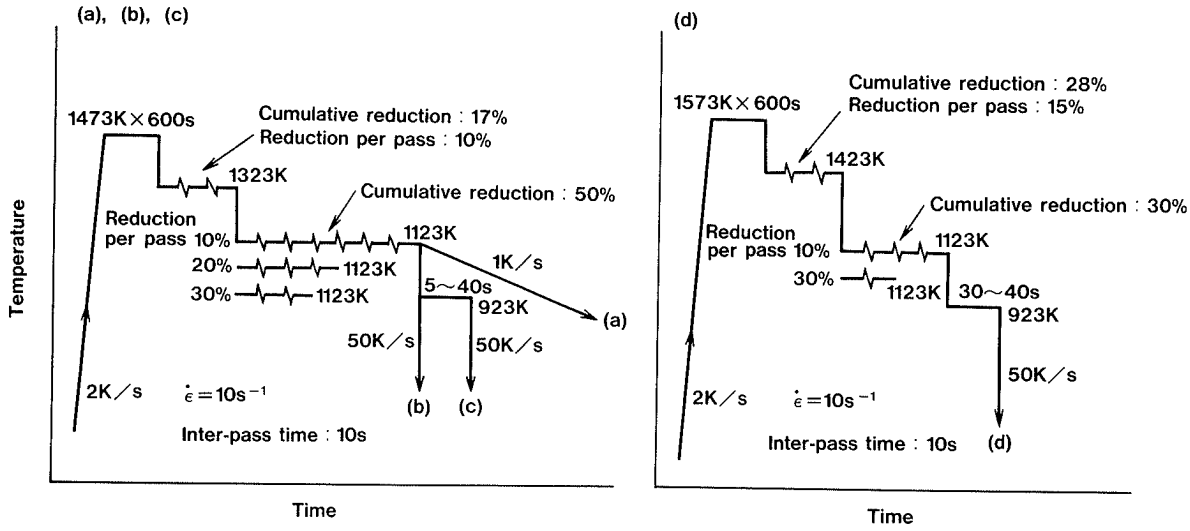

Fig. 1. Deformation conditions with hot compression device.

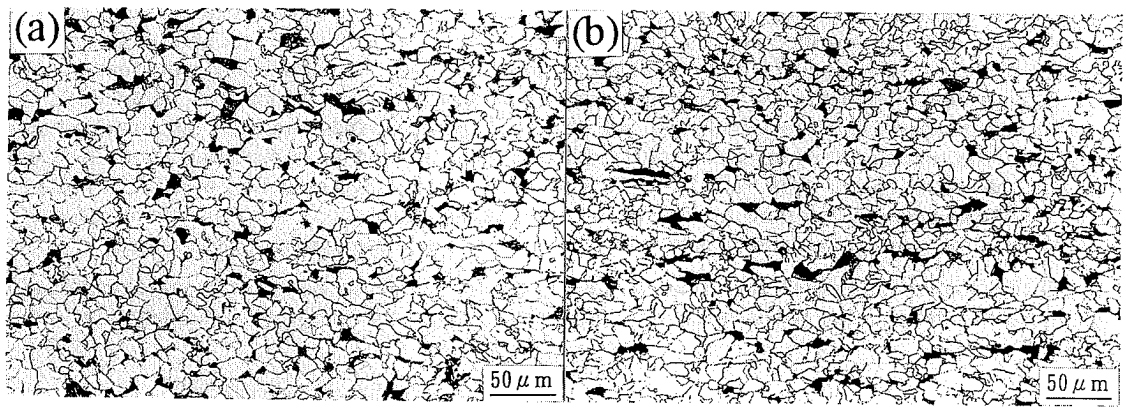

Fig. 2. Optical micrographs of steel A deformed at 1 123 K by reduction per pass of 10%, (a), or 30%, (b), under cumulative reduction of 50%.

sion device, Thermecmastor-Z (Fuji Electronic Industrial Co., Ltd). Pattern (a) in **Fig. 1** shows the deformation conditions to investigate α microstructures, $\gamma \rightarrow \alpha$ transformation temperatures (Ar_3 temperatures) and stress–strain curves. The specimens were reheated to 1 473 K and held for 600 s, then deformed at 1 323 K by the cumulative reduction of 17%, subsequently deformed at 1 123 K by the constant reduction per pass of 10% (6 passes), 20% (3 passes) or 30% (2 passes) under the cumulative reduction of 50%. The specimens were cooled at 10 s after the deformations to room temperature with the cooling rate of 1 K/s. Pattern (b) in Fig. 1 shows the deformation conditions to investigate γ microstructures through distributions of boron in γ. The specimens were quenched at 10 s after the above deformations with the cooling rate of 50 K/s. Pattern (c) in Fig. 1 shows the deformation conditions to investigate isothermal transformation behaviors. The specimens were held at 923 K for 5 to 40 s at 10 s after the above deformations and quenched with the cooling rate of 50 K/s. Pattern (d) in Fig. 1 shows the deformation conditions to investigate α nucleation behaviors. The specimens were reheated to 1 573 K and held for 600 s, then deformed at 1 423 K by the cumulative reduction of 28%, subsequently deformed at 1 123 K by the constant reduction per pass of 10% (3 passes) or 30% (1 pass) under the cumulative reduction of 30%. The specimens were held at 923 K for 30 to 40 s at 10 s after the deformations and quenched with the cooling rate of 50 K/s. In this study, the reductions mean percentage of reduced height of the specimens, the strain rate was $10\,s^{-1}$, and the each inter-pass time was 10 s.

Microstructures of the specimens were observed at the center on a central section parallel to a compression direction. Optical microscopy and scanning electron microscopy were carried out after polishing the sections and etching them in nital. Ar_3 temperatures were measured from offsets on dilatation curves in the cooling process. Distributions of boron in steel B were observed by fission track etching method.

3. Results

3.1. Influences of Reduction per Pass on α Microstructure and Ar_3 Temperature

Figure 2 shows the α microstructures of steel A deformed at 1 123 K by the reduction per pass of 10 or 30% under the cumulative reduction of 50%. The microstructures are refined with increasing the reduction per pass. **Figure 3** shows the influences of reduction per pass at 1 123 K under the cumulative reduction of 50% on the α grain size and Ar_3 temperature in steel A. The

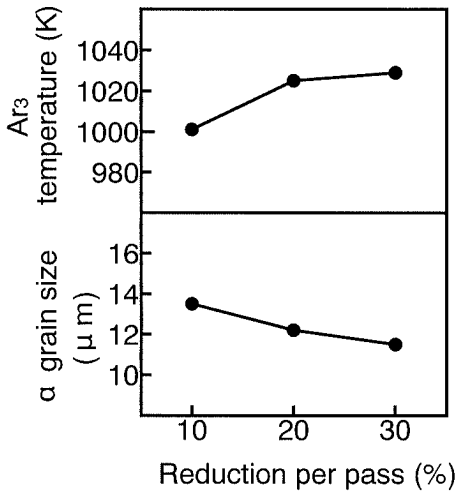

Fig. 3. Influences of reduction per pass at 1 123 K under cumulative reduction of 50% on α grain size and Ar_3 temperature in steel A.

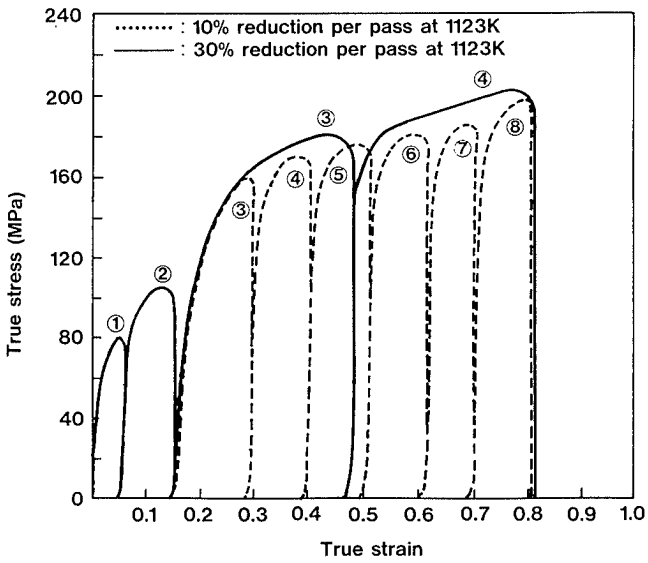

Fig. 4. Stress–strain curves of steel A deformed by conditions in pattern (a) in Fig. 1. (①, ②: Passes at 1 323 K. ③–⑧: Passes at 1 123 K.)

α grain size was measured as average diameter by the linear intersection method from Fig. 2. The α grain size is decreased about 15% with increasing the reduction per pass from 10 to 30%, while Ar_3 temperature is raised about 30 K.

3.2. Influence of Reduction per Pass on Stress–Strain Curve

Figure 4 shows the stress–strain curves of steel A deformed at 1 323 K and deformed at 1 123 K by the reduction per pass of 10 or 30% under the cumulative reduction of 50%. In the deformation at 1 123 K, the stress in 30% reduction per pass is larger than that in 10% reduction per pass, and the maximum stress at the last pass is increased about 3% with increasing the reduction per pass from 10 to 30%.

3.3. γ Microstructure in Hot Deformation

Since boron atoms can diffuse easily in heated steels because of their small size, they tend to segregate at the

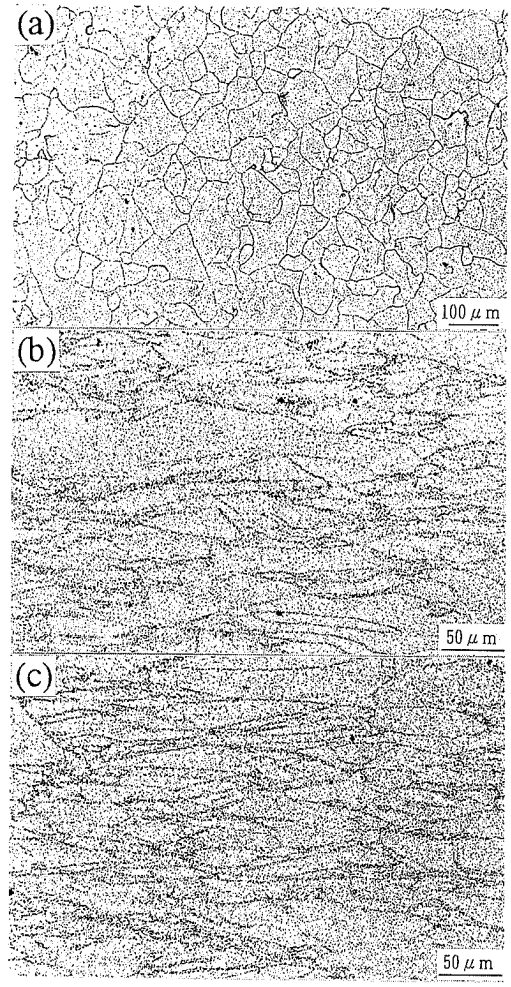

Fig. 5. Distributions of boron in steel B deformed at 1 323 K by cumulative reduction of 17%, (a), and deformed at 1 123 K by reduction per pass of 10%, (b), or 30%, (c), under cumulative reduction of 50%.

sites where iron atom alignment is strongly disordered in γ, such as γ grain boundaries, deformation bands and annealing twin boundaries. As a result, deformed prior γ structure can be observed through the distribution of segregated boron. **Figure 5** shows the distributions of boron in steel B deformed at 1 323 K by the cumulative reduction of 17% and deformed at 1 123 K by the reduction per pass of 10 or 30% under the cumulative reduction of 50%. The γ microstructure after the deformation at 1 323 K is recrystallized, and the average grain size is about 56 μm. On the other hand, the γ microstructures after the deformations at 1 123 K are elongated, and recrystallized grains are hardly observed regardless of the reduction per pass. Therefore, a deformation temperature of 1 123 K is the non-recrystallization region in the range of reduction per pass from 10 to 30% in steel B. In niobium bearing steels, it is known that recrystallization of γ is strongly retarded by strain-induced precipitation of Nb(CN).[10] In steel A and B, the amounts of niobium and nitrogen are equal to each other, but the amount of carbon is more in steel A. Since the amount of Nb(CN) in γ is increased with the amount of carbon, it is estimated that the retardation of recrystallization of γ in steel A is stronger than that in steel B. Therefore, a temperature of 1 123 K is regarded

as the non-recrystallization region also in steel A.

3.4. Influence of Reduction per Pass on Isothermal Transformation Behavior

Figure 6 shows the isothermal transformation behaviors at 923 K in steel A deformed at 1 123 K by the reduction per pass of 10 or 30% under the cumulative reduction of 50%. The α fraction transformed (F[%]) and the number of α grains (N') were measured by optical microscopy, and the α grain size (D') was calculated as the average diameter of the circles by using F and N' ($\pi(D'/2)^2=(F/100)/N'$). Though there is no significant difference in the incubation times, which are approximately 10 s in the both reduction per pass, F and N' are increased with the reduction per pass. Here, the α nucleation rate per unit area of the observed section can be estimated from the linear relation between holding time and N' at initial stage of transformation when nucleation does not saturate. Since N' at the holding time of 10 s is regarded as approximately zero in the both reduction per pass, the nucleation rate is estimated from the slope of the tie line between zero at the holding time of 10 s and N' at the holding time of 15 s. The nucleation rate is about $0.8\times10^3\,mm^{-2}s^{-1}$ in 10% reduction per pass and about $1.5\times10^3\,mm^{-2}s^{-1}$ in 30% reduction per pass. In the same way, the growth rate of α grains is estimated from the slope of the tie line between zero at the holding time of 10 s and D' at the holding time of 15 s. The growth rate is about 0.6 μm/s in the both reduction per pass.

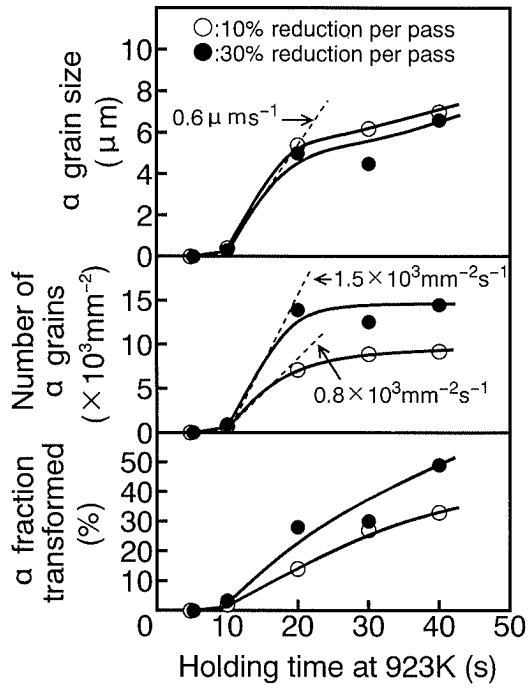

Fig. 6. Isothermal transformation behaviors at 923 K in steel A deformed at 1 123 K by reduction per pass of 10 or 30%.

3.5. Influence of Reduction per Pass on α Nucleation Behavior

The α nucleation behaviors were investigated by the deformation conditions in pattern (d) in Fig. 1. In order to distinguish between α nucleation on γ grain boundaries and that inside γ grains, the deformation conditions where the observed γ grains were larger and less elongated were selected. The holding time of 30 to 40 s at 923 K was needed to make α nucleation almost saturated. **Figure 7** shows the α nucleation in steel A deformed at 1 123 K under the cumulative reduction of 30%. α nuclei occur preferentially on the sites regarded as γ grain boundaries, deformation bands and annealing twin boundaries. The

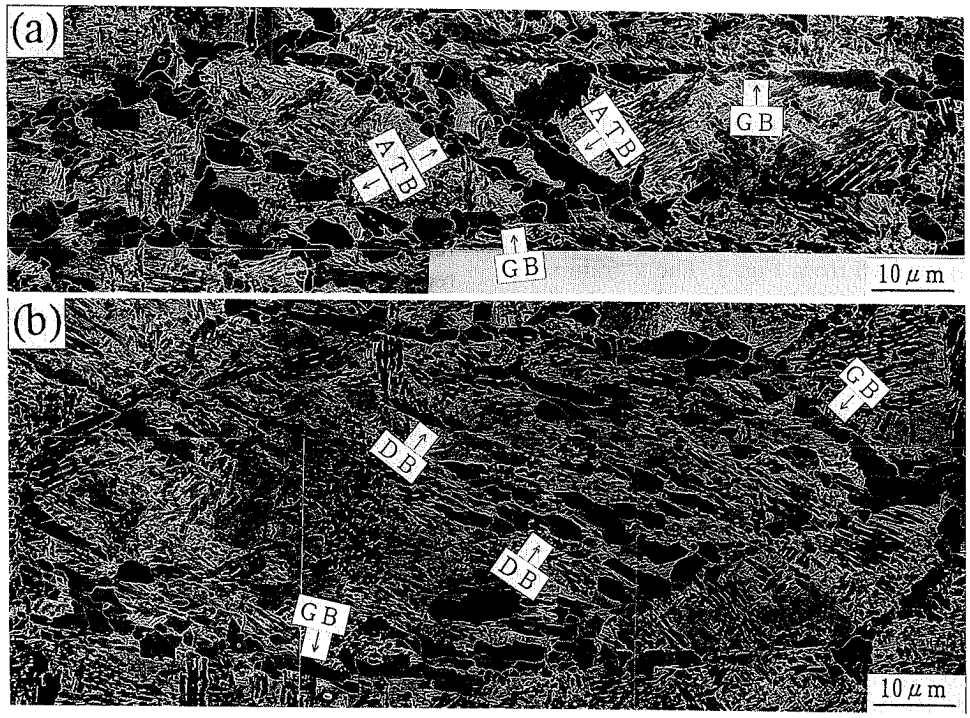

Fig. 7. Scanning electron micrographs of α nucleation at 923 K in steel A deformed at 1 123 K under cumulative reduction of 30%.
(a): α nucleation on γ grain boundaries (GB) and on annealing twin boundaries (ATB).
(b): α nucleation on GB and on deformation bands (DB).

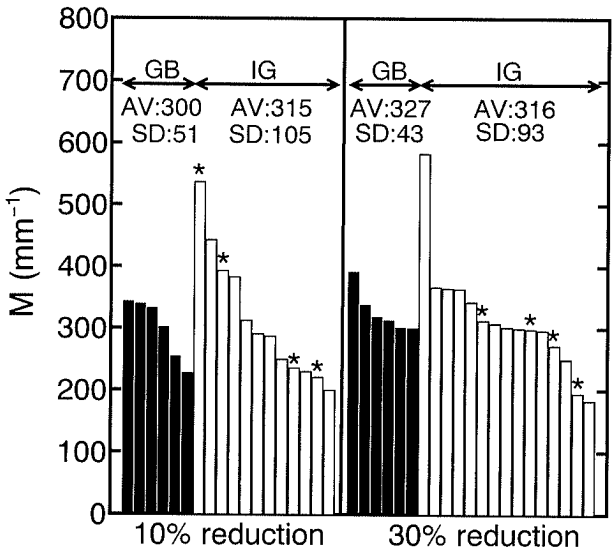

Fig. 8. Number of α nuclei per unit length of nucleation sites (M) on individual measured sites in steel A deformed at 1 123 K by reduction per pass of 10 or 30% under cumulative reduction of 30%. GB: γ grain boundaries. IG: Inside γ grains. AV: Average value. SD: Standard deviation. Marked IG (*): Annealing twin boundaries (ATB). No marked IG: Deformation bands (DB).

α nucleation sites sandwiched by parallel and straight boundaries were regarded as annealing twin boundaries,[11] and other α nucleation sites inside γ grains were regarded as deformation bands. Here, the number of α grains per unit length of saturated nucleation sites (M), which reflects activation energy for α nucleation,[12], was measured. **Figure 8** shows M on individual measured sites in steel A deformed at 1 123 K by the reduction per pass of 10 or 30% under the cumulative reduction of 30%. On γ grain boundaries, the average value of M is increased about 10% and the standard deviation of M is decreased about 16% with increasing the reduction per pass from 10 to 30%. On the other hand, inside γ grains such as on deformation bands and on annealing twin boundaries, the average value varies hardly with the reduction per pass, and the standard deviation is large in the both reduction per pass. Furthermore, there is not a remarkable difference between M on annealing twin boundaries and those on deformation bands.

4. Discussions

4.1. Mechanisms for α Grain Refinement by Large Reduction per Pass

The results in Fig. 6 indicate that the α grain refinement by the large reduction per pass in the non-recrystallization region is caused by the increase in the α nucleation rate, which corresponds to the rise in Ar_3 temperature in Fig. 3. The increase in the α nucleation rate is led by the increase in the number of α nucleation sites per unit volume (*i.e.* α nucleation site density: Nv) and/or the number of α nuclei per unit length of nucleation sites (M). Accordingly, the mechanisms for the α grain refinement is discussed by Nv and M.

4.1.1. Influence of Reduction per Pass on Nv

As mentioned above, the segregation lines of boron in

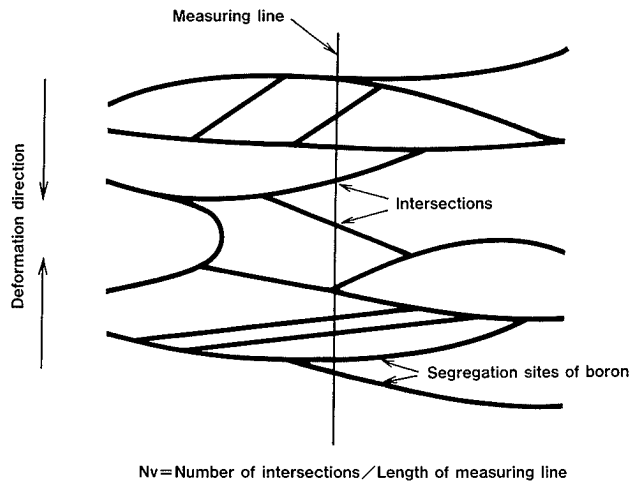

Fig. 9. Measuring method of α nucleation site density (Nv).

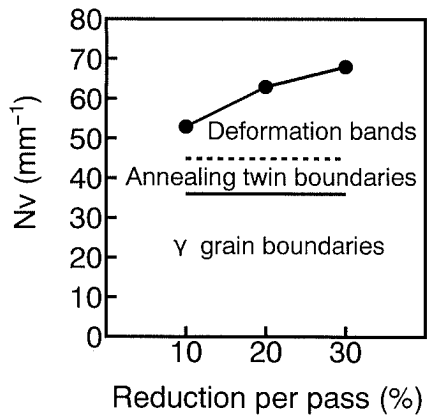

Fig. 10. Influence of reduction per pass at 1 123 K under cumulative reduction of 50% on Nv in steel B.

Figs. 5(b) and 5(c) are regarded as γ grain boundaries, deformation bands and annealing twin boundaries in deformed γ, and it is known that they act as preferential α nucleation sites.[5,6,11–15] Here, Nv is defined as the number of the segregation lines per unit length of deformation direction as shown in **Fig. 9**. **Figure 10** shows the influence of the reduction per pass at 1 123 K under the cumulative reduction of 50% on Nv in steel B. Nv is increased about 30% with increasing the reduction per pass from 10 to 30%.

It is difficult to classify the segregation lines into γ grain boundaries, deformation bands and annealing twin boundaries in Figs. 5(b) and 5(c), because the elongation of γ grains is too strong under the cumulative reduction of 50%. Therefore, Nv in Fig. 10 includes the three kinds of α nucleation sites. The number of γ grain boundaries in Nv is decided from the recrystallized γ grain size which is about 56 μm in Fig. 5(a), and from the aspect ratio of elongated γ grains which depends on the cumulative reduction of 50%. When the aspect ratio is assumed to be approximately four from the cumulative reduction of 50%, the number of γ grain boundaries in Nv is calculated to 36 mm^{-1} regardless of the reduction per pass. Furthermore, since annealing twins are formed during recrystallization process,[11,16,17] the number of annealing twin boundaries is estimated to be also regardless of the reduction per pass. Consequently, it is

Table 2. Calculations of α grain refinement (D/D_{10}) based on Eq. (5).

Red. per pass	Nv		M		N	D/D_{10}
	Nv^{GB}	Nv^{IG}	M^{GB}	M^{IG}		
10%	36	17	$M_{10}^{GB}=0.95M^{IG}$	M^{IG}	$49.5(M^{IG})^2$	1
20%	36	27	$M_{20}^{GB}=1.05M_{10}^{IG}=1.00M^{IG}$	M^{IG}	$62.8(M^{IG})^2$	0.92
30%	36	32	$M_{30}^{GB}=1.10M_{10}^{IG}=1.05M^{IG}$	M^{IG}	$71.3(M^{IG})^2$	0.89

estimated that the increase in Nv with the reduction per pass is mainly caused by the increase in deformation bands.

4.1.2. Influence of Reduction per Pass on M

On γ grain boundaries in Fig. 8, the average value of M was increased about 10% with increasing the reduction per pass from 10 to 30% under the cumulative reduction of 30%. This result indicates that γ grain boundaries were a few activated with the increase in the reduction per pass. Inside γ grains in Fig. 8, on the other hand, the average value of M was hardly affected by the reduction per pass. The values of M on annealing twin boundaries and on deformation bands may strongly depend on initial orientations of grains, consequently the scatter is large.

4.1.3. Estimation of α Grain Refinement by Increase in Nv and M

When one nucleus grows one grain in transformation, the diameter of new phase grains (D) is expressed by the following equation.[18]

$$D=(2/3N)^{1/3} \quad \text{..... (1)}$$

where, N: number of nuclei per unit volume. From the Eq. (1), grain refinement means the increase in N. In this study, the number of α grains per unit area of nucleation planes is expressed by M^2, and the number of the α nucleation planes per unit volume is Nv. Therefore, the number of α grains per unit volume (N) is expressed by the following as layers of the unit plane.

$$N=Nv\cdot M^2 \quad \text{..... (2)}$$

The decrease in α grain diameter (D) with the reduction per pass are calculated as the following by the Eqs. (1) and (2).

$$D_{20}/D_{10}=(N_{20}/N_{10})^{-1/3} \quad \text{..... (3)}$$

$$D_{30}/D_{10}=(N_{30}/N_{10})^{-1/3} \quad \text{..... (4)}$$

where, D_{10}, D_{20}, D_{30}: D under reduction per pass of 10, 20 or 30%, N_{10}, N_{20}, N_{30}: N under reduction per pass of 10, 20 or 30%.

The α grain refinement by the large reduction per pass is discussed by Nv in Fig. 10 and M in Fig. 8. Here, the α grain refinement under the cumulative reduction of 50% in the non-recrystallization region is estimated. It is assumed that the influence of the reduction per pass on M under the cumulative reduction of 50% is same with that under the cumulative reduction of 30% in Fig. 8. When the transformation is classified into that on γ grain boundaries and that inside γ grains, the Eq. (2) is modified as the following.

Table 3. Calculations of α grain refinement (D/D_{10}) based on Eq. (2).

Red. per pass	Nv	M	N	D/D_{10}
10%	53	M	$53M^2$	1
20%	63	M	$63M^2$	0.94
30%	68	M	$68M^2$	0.92

$$N=Nv^{GB}\cdot(M^{GB})^2+Nv^{IG}\cdot(M^{IG})^2 \quad \text{..... (5)}$$

where, Nv^{GB}: number of γ grain boundaries in Nv, Nv^{IG}: number of α nucleation sites inside γ grains in Nv (*i.e.* number of annealing twin boundaries and deformation bands), M^{GB}: M on γ grain boundaries, M^{IG}: M on α nucleation sites inside γ grains (*i.e.* M on annealing twin boundaries and on deformation bands). **Table 2** shows the calculations of the α grain refinement (D/D_{10}) based on the Eq. (5). The values of Nv^{GB} and Nv^{IG} were estimated from Fig. 10. The values of M^{GB} and M^{IG} were estimated from the average values in Fig. 8. The value of M^{GB} under 20% reduction per pass (M_{20}^{GB}) was assumed from the relation between M^{GB} under 10% reduction per pass (M_{10}^{GB}) and M^{GB} under 30% reduction per pass (M_{30}^{GB}) in Fig. 8. The value of M^{IG} is estimated to be regardless of the reduction per pass in Fig. 8, and the relation between M_{10}^{GB} and M^{IG} is expressed as the following.

$$M_{10}^{GB}=0.95\cdot M^{IG} \quad \text{..... (6)}$$

Therefore, M^{GB} and N are expressed by M^{IG}. On the other hand, **Table 3** shows the calculations of the α grain refinement (D/D_{10}) based on the Eq. (2). In this case, the influence of the reduction per pass on M is ignored, and M is assumed to be regardless of the reduction per pass and of the kinds of nucleation sites.

Figure 11 shows the comparison between the measurements and the calculations on the α grain refinement (D/D_{10}). The three curves were made from the values measured in Fig. 3 and the values calculated in Tables 2 and 3. When Nv^{IG} and M^{GB} are increased with the reduction per pass as shown in Table 2, D_{30}/D_{10} is calculated to be 0.89. Namely, the decrease ration of D with the increase in Nv and M is calculated to be 11%. The calculated value is close to the measured value of 15%. When M is assumed to be regardless of the reduction per pass as shown in Table 3, D_{30}/D_{10} is calculated to be 0.92. Namely, the decrease ratio of D with the increase in Nv is calculated to be 8%. Consequently, the decrease ratio of D with the increase in M is calculated to be 3%. Accordingly, it is estimated that the α grain refinement by the large reduction per

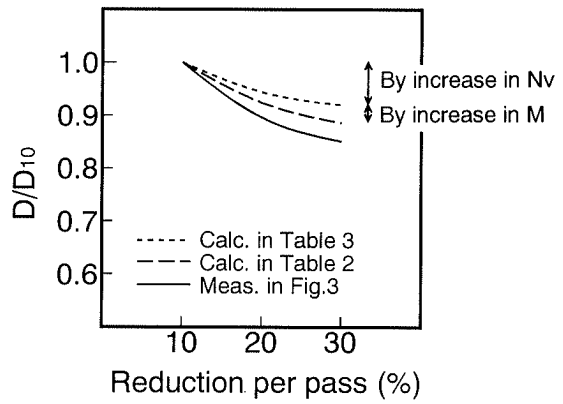

Fig. 11. Comparison between measurements and calculations on α grain refinement (D/D_{10}).

pass is mainly caused by the increase in Nv.

4.2. Mechanisms for Increase in Deformation Bands

In this study, it has been clarified that the α grain refinement by the large reduction per pass is mainly caused by the increase in Nv, which is led by the increase in deformation bands. Therefore, the mechanisms for the increase in deformation bands are discussed. Since polycrystal metals are inhomogeneously deformed because of the difference of deformation characteristics between adjacent grains, deformation bands are introduced by accommodation slip due to interactions between adjacent grains.[19,20] Deformation bands in polycrystal metals have been sometimes called micro-bands,[20] dense dislocation bands,[20] boundaries between matrix bands[21,22] and so forth, and their nature has not been fully clarified. However, since it is known that deformation bands are regions of high dislocation density,[23,24] the formation of deformation bands may be associated with the disappearance of dislocations during inter-pass and with the distribution of dislocations with deformation.

The relation between stress (σ) and dislocation density (ρ) in low carbon steels is expressed by the following equation.[25]

$$\rho = aGb(\rho - \rho_0)^{1/2} \quad \text{..... (7)}$$

where, a: constant (1.83), G: shear modulus (8×10^4 MPa), b: Burgers vector (2.6×10^{-10} m), ρ_0: initial dislocation density ($10^{12}\,m^{-2}$).[25] The dislocation density (ρ) calculated from the maximum σ at the last pass in Fig. 4 is $2.70 \times 10^{13}\,m^{-2}$ in 10% reduction per pass and $2.84 \times 10^{13}\,m^{-2}$ in 30% reduction per pass. The dislocation density (ρ) is increased only 5% with increasing the reduction per pass from 10 to 30%. As shown in pattern (a) in Fig. 1, the number of passes at 1 123 K was 6 times in 10% reduction per pass and 2 times in 30% reduction per pass under the cumulative reduction of 50%, and the each inter-pass time was 10 s. Therefore, the total inter-pass time was 50 s in 10% reduction per pass and 10 s in 30% reduction per pass. It is estimated that shortening of the total inter-pass time decreases the amount of dislocations disappearing during inter-pass, so that ρ is increased with the reduction par pass. Since deformation bands have high dislocation density, the increase in ρ may be lead to the increase in deformation bands. However, it is difficult to explain the increase in deformation bands, which is 30% of Nv in Fig. 10, by the increase in ρ, which is only 5%.

Next, the distribution of dislocations with deformation is discussed. In this case, we assume short inter-pass time, when the disappearance of dislocations does not occur but the rearrangement of dislocations occurs, constant cumulative reduction and constant ρ. In deformation by several passes, preferential deformed orientations of individual grains at latter pass may not be strictly same with those at former pass because of the rearrangement of dislocations during inter-pass. That is to say, localizing sites of dislocations may vary at each pass. Therefore, the dislocations may be more homogeneously distributed with increasing the number of passes. Paradoxically, deformation by large reduction per pass resulting in small number of passes may promote localizing of dislocations, consequently deformation bands may be easily formed. There is a necessity for the influence of reduction per pass on the formation of deformation bands to be more clarified experimentally.

5. Conclusions

In order to clarify the effects of reduction per pass in non-recrystallization temperature region of γ on α grain size of low carbon steels, isothermal hot compression tests have been performed. The hot deformations have been carried out by the constant reduction per pass of 10, 20 or 30% under the cumulative reduction of 30 or 50% in the non-recrystallization region. The main results can be summarized as follows:

(1) The α grain size is decreased about 15% with increasing the reduction per pass from 10 to 30% under the cumulative reduction of 50%. At this time, Ar_3 temperature is raised about 30 K.

(2) The α nucleation site density, which is defined as the number of γ grain boundaries, deformation bands and annealing twin boundaries per unit length of deformation direction, is increased about 30% with increasing the reduction per pass from 10 to 30% under the cumulative reduction of 50%. It is estimated that the increase in the α nucleation site density is led by the increase in deformation bands.

(3) The number of α nuclei per unit length of γ grain boundaries is increased about 10% with increasing the reduction per pass from 10 to 30% under the cumulative reduction of 30%. On the other hand, the number of α nuclei per unit length of nucleation sites inside γ grains is hardly affected by the reduction per pass.

(4) It has been clarified by the calculation that the α grain refinement by the large reduction per pass is mainly caused by the increase in the α nucleation site density.

(5) The increase in deformation bands by the large reduction per pass may be associated with shortening of total inter-pass time and with localizing of dislocations with deformation.

Acknowledgments

The authors express their appreciation to Mr. M. Tezuka, Mr. Y. Yoshida and Mr. M. Murata of Nippon

Steel Corporation, and to Dr. H. Sekine of Sekine Thermec Study for their helpful comments in this study.

REFERENCES

1) K. J. Irvine, F. B. Pickering and T. Gladman: *J. Iron Steel Inst.*, **205** (1967), No. 2, 161.
2) K. J. Irvine, T. Gladman, J. Orr and F. B. Pickering: *J. Iron Steel Inst.*, **208** (1970), No. 8, 717.
3) I. Kozasu: *Trans. Iron Steel Inst. Jpn.*, **12** (1972), 241.
4) I. Kozasu, T. Shimizu and K. Tsukada: *Trans. Iron Steel Inst. Jpn.*, **12** (1972), 305.
5) H. Sekine and T. Maruyama: *Seitetsu Kenkyu*, **289** (1976), 11920.
6) I. Kozasu, C. Ouchi, T. Sampei and T. Okita: Proc. Microalloying 75, Union Carbide Corp., New York, (1977), 120.
7) H. Sekine, T. Maruyama and M. Kawashima: *Tetsu-to-Hagané*, **60** (1974), S557.
8) H. Kaji, M. Katsumata, M. Machida and S. Kinoshita: *Tetsu-to-Hagané*, **60** (1974), S295.
9) R .Yamaba, T. Tsuzuki, Y. Tomita, N. Oyama and K. Itoh: *Tetsu-to-Hagané*, **73** (1987), 1714.
10) S. S. Hansen, J. B. Vander Sande and M. Cohen: *Metall. Trans.*, **11A** (1980), 387.
11) H. Inagaki: *Trans. Iron Steel Inst. Jpn.*, **23** (1983), 1059.
12) M. Umemoto, H. Ohtsuka and I. Tamura: Proc. Int. Conf. on Physical Metallurgy of Thermomechanical Processing of Steels and other Metals, ISIJ, (1988), 769.
13) H. Sekine and T. Maruyama: *Tetsu-to-Hagané*, **58** (1972), 1424.
14) T. M. Hoogendoorn and H. J. Spanraft: Proc. Microalloying 75, Union Carbide Corp., New York, (1977), 75.
15) R. Priestner and E. de los Rios: *Met. Technol.*, **7** (1980), 309.
16) G. Gindraux and W. Form: *J. Inst. Met.*, **101** (1973), 85.
17) W. Form, G. Gindraux and V. Mlyncar: *Met. Sci. J.*, **14** (1980), 16.
18) G. H. Gulliver: *J. Inst. Met.*, **19** (1918), 145.
19) N. Tsuji, K. Tsuzaki and T. Maki: *ISIJ Int.*, **32** (1992), 1319.
20) N. Hansen: *Mater. Sci. Technol.*, **6** (1990), 1039.
21) Y. Inokuti and R. D. Doherty: *Acta Metall.*, **26** (1978), 61.
22) Y. Uematsu, K. Hoshino, T. Maki and I. Tamura: *Tetsu-to-Hagané*, **70** (1984), 2152.
23) K. Ushioda and M. Abe: *Tetsu-to-Hagané*, **70** (1984), 96.
24) B. Bay, N. Hansen and D. Kuhlman-Wilsdorf: *Mater. Sci. Eng.*, **A113** (1989), 385.
25) A. Yoshie, T. Fujita, M. Fujioka, K. Okamoto and H. Morikawa: *Tetsu-to-Hagané*, **80** (1994), 908.